

Finite Control Set Model Predictive Torque Control Using Sliding Model Control for Induction Motors

Yanqing Zhang, *Member, IEEE*, Zhonggang Yin, *Member, IEEE*, Wei Li, Jing Liu, and Yanping Xu

Abstract—Finite control set model predictive torque control (FCS-MPTC) has become increasingly prevalent for induction motors (IM) owing to its simple concept, easy incorporation of constraints and strong flexibility. In traditional FCS-MPTC speed controller design, a classical proportional integral (PI) controller is typically chosen to generate the torque reference. However, the PI controller is dependent on system parameters and sensitive to the load torque variation, which seriously affects control performance. In this paper, a model predictive torque control using sliding mode control (MPTC + SMC) for IM is proposed to enhance the robust performance of the drive system. First, the influence of the parameter mismatches for FCS-MPTC is analyzed. Second, the shortcomings of traditional PI controller are derived. Then, the proposed MPTC + SMC method is designed, and the MPTC + PI and MPTC + SMC are compared theoretically. Finally, experimental results demonstrate the correctness and effectiveness of the proposed MPTC + SMC. In comparison with MPTC + PI, MPTC + SMC has the better dynamic performance and stronger robust performance against parameter variations and load disturbance.

Index Terms—Induction motor, Model predictive torque control, Sliding mode control, robustness.

Manuscript received April 27, 2021; revised June 10, 2021; accepted August 16, 2020. date of publication September 25, 2021; date of current version September 18, 2021.

This work was supported in part by the National Natural Science Funds of China under Grants 5217071282 and 5210071275, in part by China Postdoctoral Science Foundation under Grant 2020M683524, in part by Nature Science Basic Research Plan in Shaanxi Province under Grant 2020JQ-631 and 2021JQ-477, in part by State Key Laboratory of Electrical Insulation and Power Equipment under Grant EIPE20201, in part by State Key Laboratory of Large Electric Drive System and Equipment Technology under Grant SKLLDJ012016006, in part by Key Research and Development Project of Shaanxi Province under Grant 2019GY-060, in part by Key Laboratory of Industrial Automation in Shaanxi Province under Grant SLGPT2019KF01-12, in part by the Key R&D plan of Shaanxi Province under Grant 2021GY-282, in part by Shaanxi Outstanding Youth Fund under Grant 2020JC-40, and in part by Key Laboratory of Power Electronic Devices and High Efficiency Power Conversion in Xi'an under Grant 2019219814SYS013CG035. (*Corresponding author: Zhonggang Yin.*)

Y. Zhang, Z. Yin, and Y. Xu are with the School of Electrical Engineering, Xi'an University of Technology, Xi'an, 710048, China (email: zhangyanqing@xaut.edu.cn; zhgyin@xaut.edu.cn; xuyyp@xaut.edu.cn).

W. Li is with the VEICHI Electric Technology Co., Ltd., Suzhou, 215124, China (email: liwei19950426@163.com).

J. Liu is with the Department of Electronic Engineering, Xi'an University of Technology, Xi'an, 710048, China (email: jingliu@xaut.edu.cn).

Digital Object Identifier 10.30941/CESTEMS.2021.00030

NOMENCLATURE

| | |
|--|---|
| \mathbf{u}_s | Stator voltage vector. |
| $\boldsymbol{\psi}_s, \boldsymbol{\psi}_r$ | Stator flux linkage vector and rotor flux linkage vector. |
| $\mathbf{i}_s, \mathbf{i}_r$ | Stator current vector and rotor current vector. |
| L_s, L_r, L_m | Stator, rotor and mutual inductances. |
| T_e, T_L | Electromagnetic torque and load torque. |
| ω_e, ω_r | Electrical speed and mechanical speed. |
| R_s, R_r | Stator and rotor resistances. |
| J | Moment of inertia. |
| V_{dc} | DC bus voltage. |
| n_p | Number of pole pairs. |
| T_s | Sampling period. |

I. INTRODUCTION

INDUCTION motors (IM) are increasingly utilized in the field of industrial applications owing to high reliability, low price and other useful characteristics. However, it is nonlinear, strongly coupled and multivariable [1]. In the common control strategies for IMs, there are two different kinds of control strategies including vector control (VC) and direct torque control (DTC) [2][3]. These two control methods have obtained good performance in the field of high performance control for IMs. However, they still have some drawbacks. The robustness of vector control needs to be improved since it is of great reliance on motor parameters [4], and the torque ripple of direct torque control is quite high as the optimal switching state is chosen from a predefined switching table [5].

As an emerging control strategy, model predictive control (MPC) has been widely concerned in the past decade due to its simple concept, flexible control and straightforward handling of constraints [6-10]. Compared with VC, MPC does not need the internal current PI controller, which can directly generate expected switching signals via a cost function to drive IMs without pulse width modulation (PWM) [11]. Compared with DTC, the vector selection is more precise and effective in MPC by means of predicting the discrete-time model of IMs [12]. Therefore, MPC is regarded as a potential strategy in the field of electrical drive systems.

There are two primary classifications of MPC, i.e. the continuous control set-MPC (CCS-MPC) [13][14] and finite control set-MPC (FCS-MPC) [15][16]. In CCS-MPC, the voltage modulation is demanded to receive continuously

variable voltage vector reference, such as SVPWM. However, FCS-MPC does not require modulator. The optimal switching state is acquired directly by the online optimization of a cost function. FCS-MPC has lots of merits, such as simple concept, fast dynamics, and easy handling capability of constraints and so on. In the past decade, FCS-MPC has attracted extensive attention [17][18].

Finite control set model predictive torque control (FCS-MPTC) is a branch of FCS-MPC [19][20], in which the electromagnetic torque and the stator flux linkage magnitude are taken as the control object. The one minimizes the cost function is chosen as the optimal switching state. Therefore, FCS-MPTC selects voltage vector accurately and effectively, and it is also easy to consider multivariable control. In [19], compared with finite control set model predictive current control (FCS-MPCC), the dynamic performance of FCS-MPTC is better. Meanwhile, the torque ripple of FCS-MPTC is also lower than that of FCS-MPCC. As a result, FCS-MPTC has become a promising research focus in the domain of IM drives [21-23].

Although MPTC method has a good application prospect, there are still several aspects to be further studied to enhance its practicability, for example, the optimization design of cost function [24-28]. In the cost function design, a proper weighting factor has the significant relationship with the good control performance. However, the design of weighting factor lacks theoretical presentation currently. Therefore, a large number of experiments and simulations need to be carried out to obtain a proper weighting factor, which is time consuming and is not conducive to the further application of MPTC. [26] studies a novel MPFC control method, in which the stator flux linkage vector is used as the control object for obtaining good performance in different operating conditions. To replace complex search of weighting factors, a multi-objective fuzzy decision-making MPTC method based on priority matrix selection is investigated in [27]. In [28], the multi-objective genetic algorithm approach is introduced, which can reduce the complexity of weighting factors design to further improve the practicality of MPTC.

For improving the practicality of MPTC, another aspect that MPTC also needs to be investigated is the robustness improvement. In [29], the predictive current error with parameter uncertainties is discussed to enhance the three-phase VSI control performance. To suppress parameter mismatches and load torque disturbances, a linear disturbance observer-based PTC of induction motors is studied in [30]. [31] investigates a GPIO based PCC method to resist load torque disturbances and parameter mismatches. To solve the problem that model uncertainties may lead to larger errors in prediction behavior, an improved PCC method is studied to enhance the system robustness for PMSMs in [32].

In this paper, aiming to enhance the robustness against parameter uncertainties and load disturbance of FCS-MPTC, a MPTC + SMC method is proposed for IMs. The main contents are summarized as follows. First, FCS-MPTC with parameter mismatches is analyzed. Second, the transfer functions of PI controller with external uncertain disturbances are derived, which demonstrates that the design of PI controller needs a tradeoff between the dynamic performance and robustness.

Then, to do with this problem, the MPTC + SMC method is proposed. In addition, by introducing an adaptive reaching law in the design of SMC method, the well-known chattering phenomenon is suppressed. Finally, experimental results reveal that MPTC + SMC has the better dynamic performance and stronger robust performance against parameter variations and load disturbance than that of MPTC + PI.

II. MODELS OF INDUCTION MOTOR AND INVERTER

The dynamic equations of three-phase IM based on stationary coordinate frame $\alpha\beta$ are discussed as follows:

$$\mathbf{u}_s = R_s \mathbf{i}_s + \frac{d}{dt} \boldsymbol{\psi}_s \quad (1)$$

$$0 = R_r \mathbf{i}_r + \frac{d}{dt} \boldsymbol{\psi}_r - j\omega_r \boldsymbol{\psi}_r \quad (2)$$

$$\boldsymbol{\psi}_s = L_s \mathbf{i}_s + L_m \mathbf{i}_r \quad (3)$$

$$\boldsymbol{\psi}_r = L_r \mathbf{i}_r + L_m \mathbf{i}_s \quad (4)$$

$$T_e - T_L = \frac{J}{n_p} \frac{d\omega_r}{dt} \quad (5)$$

Reorganizing (1)-(5), the state space equations of IM are discussed as:

$$\dot{\mathbf{x}} = \mathbf{A}\mathbf{x} + \mathbf{B}\mathbf{u} \quad (6)$$

where

$$\mathbf{A} = \begin{bmatrix} -\left(\frac{R_s}{\sigma L_s} + \frac{1}{\sigma T_r}\right)\mathbf{I} + \omega_r \mathbf{J} & \frac{1}{\sigma L_s} \left(\frac{1}{T_r} \mathbf{I} - \omega_r \mathbf{J}\right) \\ -R_s \mathbf{I} & 0 \end{bmatrix},$$

$$\mathbf{B} = \begin{bmatrix} \frac{1}{\sigma L_s} \mathbf{I} & \mathbf{I} \end{bmatrix}^T, \quad \mathbf{I} = \begin{bmatrix} 1 & 0 \\ 0 & 1 \end{bmatrix}, \quad \mathbf{J} = \begin{bmatrix} 0 & -1 \\ 1 & 0 \end{bmatrix},$$

$$\mathbf{x} = [i_{s\alpha} \quad i_{s\beta} \quad \psi_{s\alpha} \quad \psi_{s\beta}]^T, \quad \mathbf{u} = [u_{s\alpha} \quad u_{s\beta}]^T,$$

$T_r = L_r/R_r$ is the time constant and $\sigma = 1 - L_m^2/L_s L_r$ is the total leakage coefficient.

The electromagnetic torque is described as:

$$T_e = 1.5n_p \text{Im}\{\boldsymbol{\psi}_s \cdot \mathbf{i}_s\} \quad (7)$$

In Fig. 1, a two-level VSI is described and the corresponding switching state \mathcal{S} and each switching signal $\mathcal{S}_a, \mathcal{S}_b, \mathcal{S}_c$ are introduced as follows:

$$\mathcal{S} = \frac{2}{3} (\mathcal{S}_a + a\mathcal{S}_b + a^2\mathcal{S}_c) \quad (8)$$

where $a = e^{j2\pi/3}$. \mathcal{S}_i are the switching states, in which $\mathcal{S}_i=1$ represents ON, $\mathcal{S}_i=0$ represents OFF, and $i = a, b, c$. The relation of the inverter output voltage vector \mathbf{u}_s and the switching signal \mathcal{S} is expressed as:

$$\mathbf{u}_s = V_{dc} \mathcal{S} \quad (9)$$

All the possible switching signals $\mathcal{S}_a, \mathcal{S}_b,$ and \mathcal{S}_c are combined, where eight switching signals and eight voltage vectors are involved. In Fig. 1(b), it is noted that $\mathbf{u}_0 = \mathbf{u}_7$, which demonstrates that it only can generate seven different voltage vectors in the complex plane.

III. ANALYSIS OF MPTC + PI WITH MISMATCHED PARAMETERS

A. Basic Principles of MPTC + PI

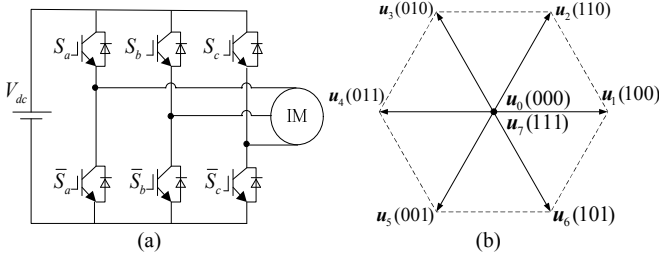


Fig. 1. (a) Two-level VSI circuit. (b) Voltage vectors in the complex plane.

In MPTC + PI algorithm of induction motor drive system, FCS-MPTC includes three primary parts: the flux linkage estimation, the stator flux linkage prediction and electromagnetic torque prediction, and the cost function minimization. Meanwhile, the predictions of stator flux linkage and electromagnetic torque should be done by each possible voltage vector. By the way, the first-order Euler discrete formula is applied. Then the predictions of \mathbf{i}_s and $\boldsymbol{\psi}_s$ can be derived as:

$$\mathbf{i}_s(k+1) = \left[1 - \left(\frac{R_s}{\sigma L_s} + \frac{1}{\sigma T_r} - j\omega_r \right) T_s \right] \mathbf{i}_s(k) + \frac{T_s}{\sigma L_s} \mathbf{u}_s(k) + \frac{T_s}{\sigma L_s} \left(\frac{1}{T_r} - j\omega_r \right) \boldsymbol{\psi}_s(k) \quad (10)$$

$$\boldsymbol{\psi}_s(k+1) = \boldsymbol{\psi}_s(k) + T_s (\mathbf{u}_s(k) - R_s \mathbf{i}_s(k)) \quad (11)$$

In view of the predictions of \mathbf{i}_s and $\boldsymbol{\psi}_s$, then T_e can be predicted as:

$$T_e(k+1) = 1.5n_p \text{Im}\{\boldsymbol{\psi}_s(k+1) \cdot \mathbf{i}_s(k+1)\} \quad (12)$$

B. Analysis of Parameters Mismatch for MPTC + PI

It is known that the predictions of stator current and flux linkage are based on the discrete model of IM, which makes the prediction procedure of FCS-MPTC dependent on motor parameters. In order to analyze the influence of parameter mismatches on the prediction accuracy, some assumptions can be made:

1) At k sampling time, the $\mathbf{i}_s(k)$ and $\boldsymbol{\psi}_s(k)$ are precise values.

2) Rotor leakage $L_{r\sigma}$ and stator leakage $L_{s\sigma}$ are constant.

The specific implementation process is:

1) Assume that R_s and L_m are the actual values.

2) The $\mathbf{i}_s(k+1)$ and $T_e(k+1)$ are predicted based on (10)-(12).

3) Assume that \tilde{R}_s and \tilde{L}_m are mismatched parameters.

4) The $\tilde{\mathbf{i}}_s(k+1)$ and $\tilde{T}_e(k+1)$ are predicted based on (13)-(15), in which $\tilde{L}_r = \tilde{L}_m + L_{r\sigma}$, $\tilde{L}_s = \tilde{L}_m + L_{s\sigma}$, $\sigma = 1 - \tilde{L}_m / \tilde{L}_s \tilde{L}_r$ and $\tilde{T}_r = \tilde{L}_r / R_r$, respectively.

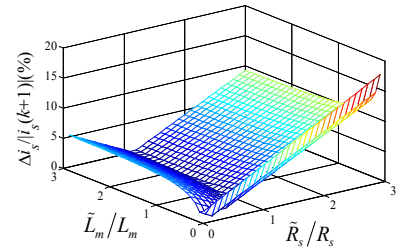
$$\tilde{\mathbf{i}}_s(k+1) = \left[1 - \left(\frac{\tilde{R}_s}{\sigma \tilde{L}_s} + \frac{1}{\sigma \tilde{T}_r} - j\omega_r \right) T_s \right] \mathbf{i}_s(k) + \frac{T_s}{\sigma \tilde{L}_s} \mathbf{u}_s(k) + \frac{T_s}{\sigma \tilde{L}_s} \left(\frac{1}{\tilde{T}_r} - j\omega_r \right) \boldsymbol{\psi}_s(k) \quad (13)$$

$$\tilde{\boldsymbol{\psi}}_s(k+1) = \boldsymbol{\psi}_s(k) + T_s (\mathbf{u}_s(k) - \tilde{R}_s \mathbf{i}_s(k)) \quad (14)$$

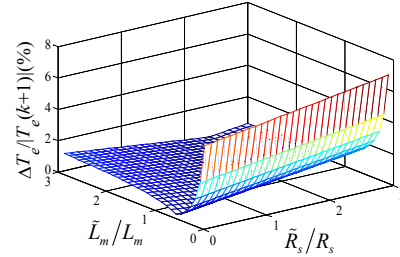
$$\tilde{T}_e(k+1) = 1.5n_p \text{Im}\{\tilde{\boldsymbol{\psi}}_s(k+1) \cdot \tilde{\mathbf{i}}_s(k+1)\} \quad (15)$$

5) The prediction errors of \mathbf{i}_s and T_e are defined as $\Delta \mathbf{i}_s = |\tilde{\mathbf{i}}_s(k+1) - \mathbf{i}_s(k+1)|$, $\Delta T_e = |\tilde{T}_e(k+1) - T_e(k+1)|$, respectively.

Supposing that IM operates in rated state, and the direction of stator flux linkage $\boldsymbol{\psi}_s$ only is related to α axis. In this paper, based on the IM parameters, $\mathbf{i}_s = 4.1e^{j(\pi/3)}$, $\boldsymbol{\psi}_s = 0.95e^{j0}$ are true at this instant. A two-level VSI products eight voltage vectors, which results in lots of analysis conditions in parameter mismatches. To simplify the analysis process, the one that maximizes prediction error is chosen as used switching state at k sampling instant in this paper. In Fig. 2(a), the prediction error of \mathbf{i}_s is illustrated when R_s and L_m are different from the true values. When $\tilde{L}_m/L_m = 1$ and $\tilde{R}_s/R_s = 1$, the prediction error of \mathbf{i}_s is 0. Moreover, the error of \mathbf{i}_s is susceptible to mismatched L_m . It shows that the prediction error of \mathbf{i}_s is quite larger when $\tilde{L}_m/L_m < 1$. Fig. 2(b) shows the prediction error of T_e when R_s and L_m are different from the true values. It can be concluded that the effect of parameter mismatches on the prediction errors of \mathbf{i}_s and T_e possess the identical trends.



(a)



(b)

Fig. 2. (a) Stator current prediction error with mismatched R_s and L_m . (b) Electromagnetic torque prediction error with mismatched R_s and L_m .

C. Analysis of Uncertain Disturbances for MPTC + PI

To simplify the analysis process, traditional MPTC + PI can be simplified as in Fig.3, in which the transfer function of PI controller is expressed as (16), where k_p is the proportional coefficient and k_i is the integral coefficient.

$$F(s) = k_p + \frac{k_i}{s} \quad (16)$$

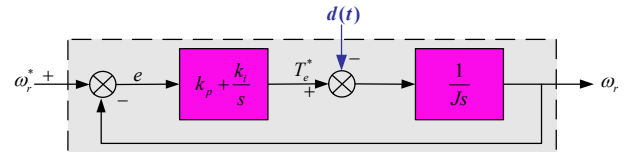


Fig. 3. The simplified block diagram of MPTC + PI.

The transfer function of the induction motor is:

$$G(s) = \frac{1}{Js} \quad (17)$$

Fig. 3 shows the transfer function $G_c(s)$ and the disturbance transfer function $G_d(s)$, which are described as (18) and (19):

$$G_c(s) = \frac{\omega_r(s)}{\omega_r^*(s)} \Big|_{d(t)=0} = \frac{k_p}{J} \frac{s + (k_i/k_p)}{s^2 + (k_p/J)s + (k_i/J)} \quad (18)$$

$$G_d(s) = \frac{\omega_r(s)}{d(s)} \Big|_{\omega_r^*=0} = -\frac{1}{J} \frac{s}{s^2 + (k_p/J)s + (k_i/J)} \quad (19)$$

It can be concluded that both the speed transient capability and the disturbance rejection capability are based on the denominator $s^2 + (k_p/J)s + (k_i/J)$. Meanwhile, it can be rewritten as:

$$s^2 + 2\zeta\omega_0s + \omega_0^2 \quad (20)$$

where ζ ($\zeta = k_p/(2\sqrt{Jk_i})$) is the damping ratio and ω_0 ($\omega_0 = \sqrt{k_i/J}$) is the undamped natural frequency. The induction motor runs at underdamping state when $0 < \zeta < 1$. Meanwhile, $\zeta = 1$ indicates that IM functions at critically damping state. When $\zeta > 1$, the IM runs at overdamping state.

To analyze the anti-disturbance ability of the PI controller, the load disturbance step $\Delta d(t)$ is taken into account. As shown in (21), the integer error (IE) can be described as:

$$IE = \int_0^\infty edt = -\lim_{s \rightarrow 0} G_d(s) \frac{\Delta d(t)}{s} = \frac{\Delta d(t)}{J} \left(\frac{2\zeta J}{k_p} \right)^2 \quad (21)$$

It can be concluded that a small value of ζ will improve the anti-disturbance ability of the PI controller. However, too small value of ζ may result in the system instability. Thus, for the PI controller, there exists a tradeoff between the anti-disturbance capability and the speed dynamic response.

IV. THE PROPOSED MPTC + SMC

A. Fundamental Principles of MPTC + SMC

The prediction error of MPTC + PI with parameter mismatches is inevitable. As analyzed in section III, the design of PI controller in MPTC needs a compromise between speed dynamic response and disturbance rejection capability, which will eventually result in the weak robustness of control system, especially in sudden load torque changes and parameter mismatches. Therefore, for improving the robustness of IM, a MPTC + SMC method is proposed in this paper. Traditionally, PI controller is used in the drive system. The proposed method, MPTC + SMC, uses the SMC controller as speed outer loop. It has the advantage of improving the robustness of control system due to its insensitivity to external disturbances and mismatched parameters. The block diagram of MPTC + SMC is expressed in Fig. 4.

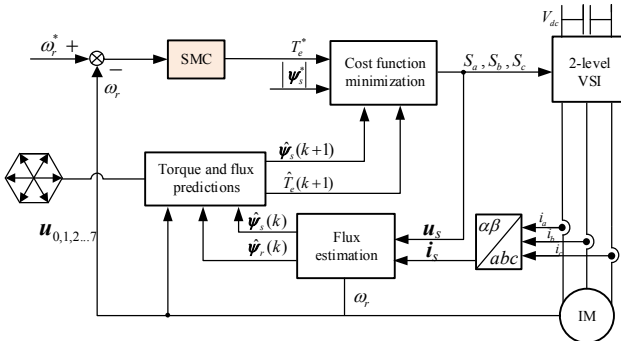


Fig. 4. The block diagram of MPTC + SMC for IM.

The basic idea of sliding mode control is that any point on the state space continually traverses the sliding mode surface, and insures that the IM is gradually stable on the sliding mode surface. Since the sliding mode controller is adopted as the speed outer loop controller in this paper, the state variables are described as:

$$\begin{cases} x_1 = \omega_r^* - \omega_r \\ x_2 = \dot{x}_1 = -\dot{\omega}_r \end{cases} \quad (22)$$

where ω_r^* is the given speed.

Combining (5) and (22), it can be derived that:

$$\begin{cases} \dot{x}_1 = -\dot{\omega}_r = -(n_p/J)(T_e - T_L) \\ \dot{x}_2 = -\ddot{\omega}_r = -(n_p/J)\dot{T}_e \end{cases} \quad (23)$$

Assuming that $b = n_p/J$, $\tau = n_p T_L/J$ and $U = \dot{T}_e$, then (23) can be rewritten as:

$$\begin{bmatrix} \dot{x}_1 \\ \dot{x}_2 \end{bmatrix} = \begin{bmatrix} 0 & 1 \\ 0 & 0 \end{bmatrix} \begin{bmatrix} x_1 \\ x_2 \end{bmatrix} + \begin{bmatrix} 0 \\ -b \end{bmatrix} U \quad (24)$$

The first-order sliding mode surface is designed as:

$$s = cx_1 + x_2 \quad (25)$$

where c is the sliding mode coefficient.

For convenience of analysis, the sliding control law is designed as:

$$U = \varphi_1 x_1 + \varphi_2 x_2 \quad (26)$$

where φ_1 and φ_2 are constants, respectively.

To make the control system stable, then $ss' < 0$. It can be organized as:

$$ss' = (cx_1 + x_2)s = \left[c\left(1 - \frac{b}{c}\varphi_2\right)x_2 - b\varphi_1 x_1 \right] s < 0 \quad (27)$$

Thus it can be derived that:

$$\begin{cases} \varphi_1 = \begin{cases} \alpha_1 > 0 & x_1 s > 0 \\ \beta_1 < 0 & x_1 s < 0 \end{cases} \\ \varphi_2 = \begin{cases} \alpha_2 < c/b & x_2 s > 0 \\ \beta_2 > c/b & x_2 s < 0 \end{cases} \end{cases} \quad (28)$$

where α_1 , α_2 , β_1 and β_2 are constants, respectively.

According to (28), the ultimate control variable T_e^* is expressed as:

$$T_e^* = \frac{1}{s}(\varphi_1 x_1 + \varphi_2 x_2) = \varphi_2 x_1 + \varphi_1 \left(\frac{1}{s} x_1 \right) \quad (29)$$

B. Stability Analysis of MPTC + SMC

In this paper, the Lyapunov stability theory is adopted, in which the Lyapunov function $V(x)$ is selected as:

$$V(x) = \frac{1}{2} s^2 \quad s \neq 0 \quad (30)$$

Based on (30), it can be derived that:

$$\dot{V}(x) = s\dot{s} \quad s \neq 0 \quad (31)$$

Due to the Lyapunov stability theory, since $ss' < 0$, then $\dot{V}(x) < 0$, and the IM control system is stable.

Making the sliding mode surface $s=0$, it can be concluded that:

$$s = cx_1 + x_2 = cx_1 + \dot{x}_1 = 0 \quad (32)$$

By solving (32), it can be derived that:

$$x_1 = \omega_r^* - \omega_r = C_0 e^{-\frac{t}{c}} \quad (C_0 \text{ is a constant}) \quad (33)$$

From (33), when $t \rightarrow \infty$, x_1 is convergent to zero. The control performance is completely determined by c , which is unrelated to motor parameters and external disturbances. Furthermore, the required time of the system stability is only related to c , hence, it has better robustness and rapidity. However, due to the limits of some factors, such as time delay, space lag, the parameters of SMC controller need to be compromised in the implementation of control system.

C. Comparison of MPTC + PI and MPTC + SMC controllers

For convenient analysis, (34) and (35) are supplemented. In MPTC + PI, T_e^* can be obtained as:

$$T_e^* = k_p x_1 + k_i \left(\frac{1}{s} x_1 \right) \quad (34)$$

Associating (5) with (15), it can be derived that:

$$\ddot{x}_1 + bk_p \dot{x}_1 + bk_i x_1 - \tau = 0 \quad (35)$$

In this section, the comparisons between MPTC + PI and MPTC + SMC will be elaborated by three aspects: 1) the complexity of parameter tuning, 2) the complexity of controller implementation, and 3) the disturbance rejection ability.

1) The complexity of parameter tuning

It can be seen from (35) that the IM system based on MPTC + PI is a second-order system. Hence, if k_p and k_i in the MPTC + PI are selected properly, then the drive system keeps steady. Nevertheless, the tuning process of MPTC + PI is relatively complicated. In the proposed MPTC + SMC, the induction motor is reduced to a first-order system, which means that if c is selected appropriately, then the stability of the control system can be guaranteed.

2) The complexity of controller implementation

According to (29) and (34), the expressions of the two controllers are extremely similar. Therefore, MPTC + SMC does not increase the implementation complexity. It can be seen that MPTC + SMC is the variable structure control, and its control quantity depends on the value of φ_1 , φ_2 . The change of φ_1 and φ_2 is determined by the stability of control system and the sliding mode surface.

3) The disturbance rejection ability

If the external disturbance $d(t)$ occurs in MPTC + PI, the control system performance will be affected from (35) if the previous parameters remain constant. However, it can be seen that the selection of MPTC + SMC parameters is not altered, and the control performance is not affected. The values of φ_1 and φ_2 are limited to a certain range. Hence, when the motor parameters are varying, the control system performance will not be influenced as long as φ_2 is in a reasonable range. However, in the implementation of control system, due to the limits of time delay, space lag and so on, it must be a tradeoff in the design of controller parameters for SMC controller.

D. Chattering Suppression of MPTC + SMC

In this paper, to suppress the inherent chattering problem, an adaptive reaching law is designed, which is expressed as:

$$\begin{cases} \dot{s} = -k_1 |s|^\alpha \operatorname{sgn}(s) - \varepsilon' \operatorname{sgn}(s) \\ \varepsilon' = k_2 \tan \operatorname{sig}|x| \end{cases} \quad (36)$$

where $k_1 > 0$, $\alpha > 0$, $k_2 > 0$ and $\tan \operatorname{sig}|x| = \frac{1 - e^{-|x|}}{1 + e^{-|x|}}$. Based on (24), (25) and (36), T_e^* can be derived as:

$$T_e^* = \frac{1}{b} \int [cx_2 + k_1 |s|^\alpha \operatorname{sgn}(s) + \varepsilon' \operatorname{sgn}(s)] dt \quad (37)$$

According to the aforementioned, in Fig. 5, the control block diagram of SMC algorithm is described.

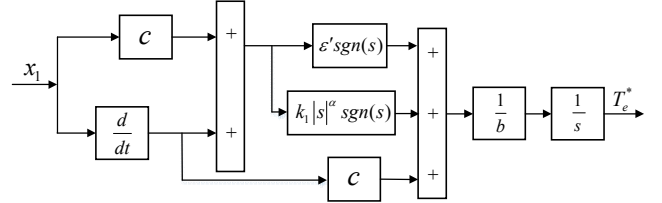


Fig. 5. The control block diagram of SMC algorithm.

E. Flux linkage Estimation

The appropriate operation of MPTC + SMC relies on accurate estimation of the flux linkage, which is carried out by an adaptive full-order observer.

$$\dot{\hat{x}} = \mathbf{A}\hat{x} + \mathbf{B}u + \mathbf{G}(\hat{i}_s - \hat{i}_s^*) \quad (38)$$

where $\hat{x} = [\hat{i}_s \quad \hat{\psi}_s]^T$.

Generally, the design of \mathbf{G} is significant, and a simple feedback gain matrix \mathbf{G} is shown in (39), in which the specific theoretical analysis is noted in [16].

$$\mathbf{G} = \begin{bmatrix} 2\eta \\ \eta/(\lambda L_r) \end{bmatrix} \quad (39)$$

where η is a negative constant.

F. Predictions of Stator Flux linkage and Electromagnetic Torque

The $\hat{\psi}_s(k+1)$ and $\hat{T}_e(k+1)$ in MPTC + SMC can be predicted as:

$$\hat{\psi}_s(k+1) = \hat{\psi}_s(k) + T_s u_s(k) - R_s T_s \hat{i}_s(k) \quad (40)$$

$$\|\hat{\psi}_s(k+1)\| = \sqrt{\hat{\psi}_{s\alpha}(k+1)^2 + \hat{\psi}_{s\beta}(k+1)^2} \quad (41)$$

$$\hat{T}_e(k+1) = 1.5p \operatorname{Im}\{\hat{\psi}_s(k+1)\hat{i}_s^*(k+1)\} \quad (42)$$

To eliminate the impact of the well-known one-step delay in digital control system, the two-step prediction is generally used. Therefore, the cost function is constructed as follows:

$$g = |T_e^* - \hat{T}_e(k+2)| + k_v \|\psi_s^* - |\hat{\psi}_s(k+2)\| \quad (43)$$

where k_v is the weighting factor, which increases or decreases the relative importance of the torque versus flux control in MPTC system. If the same importance is assigned to both control objectives, this factor would correspond to the ratio between the nominal magnitudes of the torque T_n and stator flux $|\psi_{sn}|$, which is shown as

$$k_{\psi} = \frac{T_n}{|\psi_{sn}|} \quad (44)$$

To implement the control algorithm of MPTC + SMC, the total flow diagram is presented in Fig. 6.

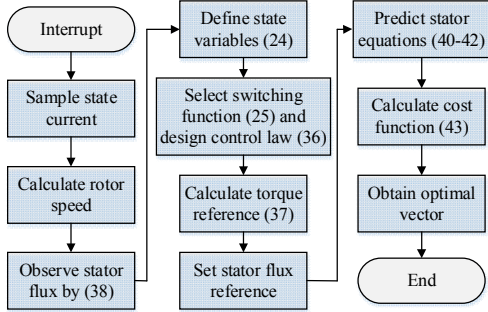


Fig. 6. The total flow diagram of the control algorithm of MPTC + SMC.

V. EXPERIMENTAL RESULTS

A. Description of the Experimental Platform

To verify the correctness and effectiveness of the proposed MPTC + SMC, some experiments have been implemented. Table I shows the induction motor parameters. The experimental platform is presented in Fig. 7, which mainly includes main circuit, control board, a loading system and the IM. In addition, the loading system consists of a servo inverter and a PMSM. The TI TMS320F28335 DSP is used as the main processor. A 4-channel digital-to-analog inverter chip is also extended on the main circuit for internal variable observation.

TABLE I
PARAMETERS OF INDUCTION MOTOR

| Parameter | Value | Parameter | Value |
|----------------|-------|--------------------|-------|
| rated power/kW | 1.1 | rated voltage/V | 380 |
| R_s/Ω | 5.27 | rated current/A | 2.9 |
| R_r/Ω | 5.07 | rated frequency/Hz | 50 |
| L_s/H | 0.479 | rated torque/N·m | 7.45 |
| L_r/H | 0.479 | pole pair | 2 |
| L_m/H | 0.421 | $J/kg \cdot m^2$ | 0.02 |

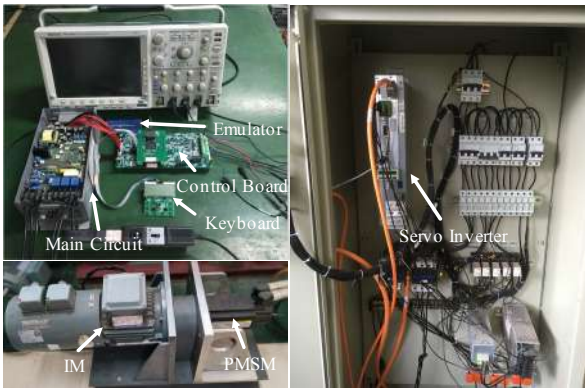


Fig. 7. Experimental platform.

B. Overall Performance

Fig. 8 shows the overall control performance of the proposed MPTC + SMC, in which the induction motor operates from standstill to the rated speed. From top to bottom, the waveforms

are speed, electromagnetic torque, a-phase stator current and stator flux linkage amplitude, respectively. It is visible that the rotor speed is stable and smooth, in addition, the current is sinusoidal in shape and the magnitude of stator flux linkage is constant. Therefore, it shows that the proposed MPTC + SMC has good dynamic and steady-state performances.

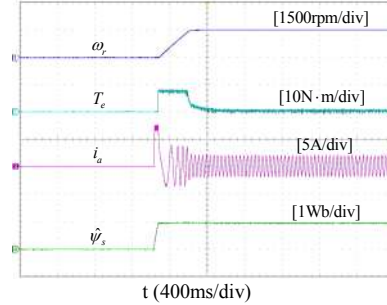


Fig. 8. MPTC + SMC response from 0 to 1500rpm.

Fig.9 shows the results of speed reversal responses from 1500rpm to -1500rpm, in which the IM is enforced to reverse direction during operation. From the dynamic response procedure of the speed reversion, the rotor speed is smoothly switched, the stator current is sinusoidal in shape, and the amplitude of stator flux linkage remains constant. It reveals that the proposed method presents the satisfactory dynamic performance.

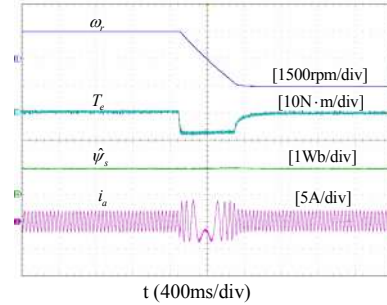


Fig. 9. MPTC + SMC response in the speed reversal process.

Fig.10 shows the transient performance of α -phase stator flux linkage and the β -phase stator flux linkage. It concludes that the stator flux linkage curves are smooth during the speed reversal process. α -phase stator flux linkage and the β -phase stator flux linkage estimation are also quite accurate, thus it can achieve satisfactory performance in the transient response.

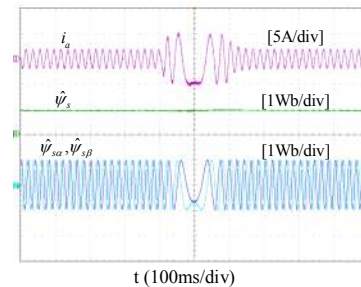


Fig. 10. Stator flux linkage waveforms in the process of a speed reversal process.

C. Dynamic Performance

To demonstrate the disturbance rejection ability, Fig. 11 shows the comparison results when the IM operates at 1500 rpm with the rated load. From top to bottom, the waveforms are speed, electromagnetic torque, stator flux linkage amplitude and a-phase stator current, respectively. As shown in Fig. 11(a), the speed drop of MPTC + PI is 300 rpm and the recovery time is 0.6s. Compared with MPTC + PI, the speed drop of the proposed MPTC + SMC is reduced by 70rpm and the recovery time is decreased by 0.15s in Fig. 11(b). In conclusion, it indicates that MPTC + SMC has the better performance against disturbance rejection ability than MPTC + PI.

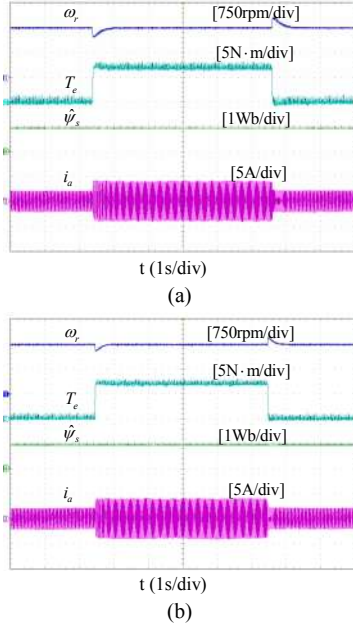


Fig. 11. Comparison of loading capability for (a) MPTC + PI (b) MPTC + SMC.

To verify the dynamic response, the torque step response has been carried out in Fig. 12. From top to bottom, the waveforms are electromagnetic torque reference and electromagnetic torque, respectively. When the step load is suddenly added from 0 to 7.45 N·m at 1500 rpm, the rising time of electromagnetic torque for MPTC + PI is 41ms. However, the rising time of electromagnetic torque for MPTC + SMC is 30ms. Therefore, it reveals that the proposed MPTC + SMC has the faster dynamic torque response than that of MPTC + PI.

D. Robust Performance under Parameter Mismatch

To verify the robust performance, the change of the motor parameters is considered. Fig 13 reveals the comparisons of experimental results for MPTC + PI and MPTC + SMC. Fig 13(a) indicates the experimental result with stator resistance deviation $|\Delta R_s| = 30\%$ at 30 rpm for MPTC + PI. When the stator resistance is suddenly changed by 30%, the rotor speed ω_r has a larger oscillation, and the a-phase stator current i_a becomes poor and is not sinusoidal. Fig 13(b) indicates the experimental result with stator resistance deviation $|\Delta R_s| = 30\%$ at 30rpm for MPTC + SMC. For MPTC + SMC, the rotor speed has a slight fluctuation, and the a-phase stator current waveform keeps sinusoidal after a short period of adjustment. In a word, it

reveals that the proposed MPTC + SMC has the stronger robustness to stator resistance deviation than MPTC + PI.

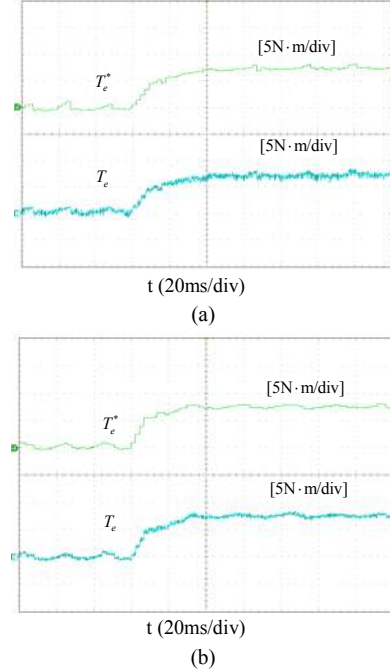


Fig. 12. Comparison of dynamic responses for (a) MPTC + PI (b) MPTC + SMC.

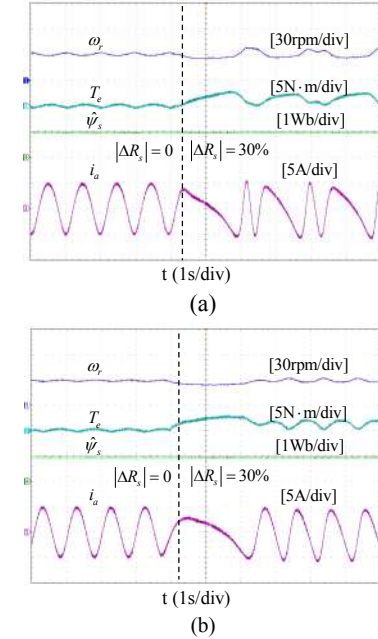


Fig. 13. Comparison results with R_s deviation for (a) MPTC + PI (b) MPTC + SMC.

Similarly, Fig. 14 reveals the experimental comparisons of MPTC + PI and the proposed MPTC + SMC with mutual inductance deviation $|\Delta L_m| = 30\%$ at 30 rpm. When the mutual inductance is suddenly changed by 30%, for MPTC + PI, the rotor speed ω_r and the a-phase stator current i_a waveforms have much larger fluctuations than that of MPTC + SMC. In addition, it indicates that both MPTC + PI and MPTC + SMC can make the control system stable. However, the robust performance of MPTC + SMC to mutual inductance deviation is better than MPTC + PI.

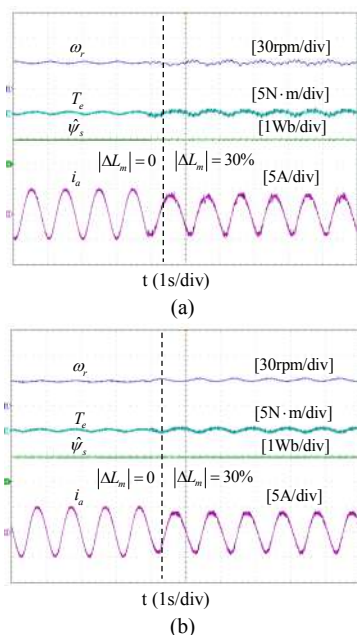


Fig. 14. Comparison results with L_m deviation for (a) MPTC + PI (b) MPTC + SMC.

VI. CONCLUSION

A finite control set model predictive torque control using sliding model control for induction motors is proposed in this paper. By analyzing the influence of MPTC + PI with mismatched parameters, the prediction error of MPTC + PI can not be avoided. Then, to enhance the robust performance of the control system, the SMC controller is proposed as speed outer loop for FCS-MPTC. Furthermore, to weaken the chattering problem of SMC controller, an adaptive reaching law is designed. The experimental results demonstrate the effectiveness of the proposed MPTC + SMC, and it indicates that MPTC + SMC not only has good dynamic and steady-state performances, but also has stronger robustness against load disturbance and parameter variations.

REFERENCES

- [1] Z. Yin, Y. Zhang, C. Du, J. Liu, X. Sun, and Y. Zhong, "Research on anti-error performance of speed and flux estimation for induction motors based on robust adaptive state observer," *IEEE Trans. Ind Electron.*, vol. 63, no. 3, pp. 3499-3510, Jun. 2016.
- [2] A. B. Luis, L. C. Jesus, and L. C. Eduardo, "Speed and position controllers using indirect field-oriented control: a classical control approach," *IEEE Trans. Ind Electron.*, vol. 61, no. 4, pp. 1928-1943, Apr. 2014.
- [3] X. T. Garcia, A. Arias, M. G. Jayne, and P. I. A. Witting, "Direct torque control of induction motors utilizing three-level voltage source inverters," *IEEE Trans. Ind Electron.*, vol. 55, no. 5, pp. 956-958, Feb. 2008.
- [4] Z. Yin, G. Li, Y. Zhang, and J. Liu, "Symmetric strong tracking extended kalman filter based sensorless control of induction motor drives for modeling error reduction," *IEEE Trans. Ind Informat.*, vol. 15, no. 2, pp. 650-662, Feb. 2019.
- [5] C. Lascu, S. Jafarzadeh, M. S. Fadali and F. Blaabjerg, "Direct torque control with feedback linearization for induction motor drives," *IEEE Trans. Power Electron.*, vol. 32, no. 3, pp. 2072-2080, Mar. 2017.
- [6] M. Siami, D. A. Khaburi, and J. Rodriguez, "Torque ripple reduction of predictive torque control for PMSM drives with parameter mismatch," *IEEE Trans. Power Electron.*, vol. 32, no. 9, pp. 7160-7168, Sep. 2017.

- [7] Y. Zhang, H. Yang, "Model predictive torque control of induction motor drives with optimal duty cycle control," *IEEE Trans. Power Electron.*, vol. 29, no. 12, pp. 6593-6603, Dec. 2014.
- [8] Y. Zhang, H. Yang, "Model predictive flux control of induction motor drives with switching instant optimization," *IEEE Trans. Energy Convers.*, vol. 30, no. 3, pp. 1113-1122, Sep. 2015.
- [9] Y. Zhang, D. Xu, J. Liu, S. Gao, and W. Xu, "Performance improvement of model predictive current control of permanent magnet synchronous motor drives," *IEEE Trans. Ind Appl.*, vol. 53, no. 4, pp. 3683-3695, Jul. 2017.
- [10] Z. Zhang, J. Rodriguez, and R. Kennel, "Advanced control strategies for direct-drive PMSG wind turbine systems: direct predictive torque control approaches," *CPSS Trans. Power. Electron. and Appl.*, vol. 2, no. 3, pp. 217-225, Sep. 2017.
- [11] J. Rodriguez, R. Kennel, J. R. Espinoza, M. Trincado, C. A. Silva, and C. A. Rojas, "High-performance control strategies for electrical drives: an experimental assessment," *IEEE Trans. Ind. Electron.*, vol. 59, no. 2, pp. 812-820, Feb. 2012.
- [12] K. Jezernik, J. Korelic, and R. Horvat, "PMSM sliding mode FPGA-based control for torque ripple reduction," *IEEE Trans. Power Electron.*, vol. 28, no. 7, pp. 3549-3556, Jul. 2013.
- [13] Z. Yin, X. Han, C. Du, J. Liu, and Y. Zhong, "Research on model predictive current control for induction machine based on immune-optimized disturbance observer," *IEEE J. Emerg. Sel. Topics Power Electron.*, vol. 6, no. 4, pp. 1699-1710, Dec. 2018.
- [14] S. Mariethoz, A. Domahidi, and M. Morari, "High bandwidth explicit model predictive control of electrical drives," *IEEE Trans. Ind Appl.*, vol. 48, no. 6, pp. 1980-1992, Nov. 2012.
- [15] J. Rodriguez, "Model predictive control-a review of its applications in power electronics," *IEEE Ind. Electron. Magaz.*, pp. 17-30, Mar. 2014.
- [16] Y. Zhang, H. Yang, "Two-vector-based model predictive torque control without weighting factors for induction motor drives," *IEEE Trans. Power Electron.*, vol. 31, no. 2, pp. 1381-1390, Feb. 2016.
- [17] F. Wang, J. Wang, R. Kennel, and J. Rodriguez, "Fast speed control of AC machines without the proportional-integral controller: using an extended high-gain state observer," *IEEE Trans. Power Electron.*, vol. 34, no. 9, pp. 9006-9015, Sep. 2019.
- [18] A. A. Ahmed, B. K. Koh, H. S. Park, K.B. Lee, and Y. H. Lee, "Finite-control set model predictive Control method for torque control of induction motors using a state tracking cost index," *IEEE Trans. Ind. Electron.*, vol. 64, no. 3, pp. 1916-1928, Mar. 2017.
- [19] F. Wang, S. Li, X. Mei, W. Xie, J. Rodriguez, and R. Kennel, "Model-based predictive direct control strategies for electrical drives: an experimental evaluation of PTC and PCC methods," *IEEE Trans. Ind Informat.*, vol. 11, no. 3, pp. 671-681, Jun. 2015.
- [20] F. Wang, Z. Chen, P. Stolze, J. F. Stumper, J. Rodriguez, and R. Kennel, "Encoderless finite-state predictive torque control for induction machine with a compensated MRAS," *IEEE Trans. Ind Informat.*, vol. 10, no. 2, pp. 1097-1106, May. 2014.
- [21] W. Xie, X. Wang, F. Wang, W. Xu, R. Kennel, and D. Gerling, "Dynamic loss minimization of finite control set-model predictive torque control for electric drive system," *IEEE Trans. Power Electron.*, vol. 31, no. 1, pp. 849-859, Jan. 2016.
- [22] Y. Zhang, D. Xu, and L. Huang, "Generalized multiple-vector-based model predictive control for PMSM drives," *IEEE Trans. Ind. Electron.*, vol. 65, no. 12, pp. 9356-9366, Dec. 2018.
- [23] H. Miranda, P. Cortes, J. I. Yuz, and J. Rodriguez, "Predictive torque control of induction machines based on state-space models," *IEEE Trans. Ind. Electron.*, vol. 56, no. 6, pp. 1916-1924, Jun. 2009.
- [24] M. Norambuena, J. Rodriguez, Z. Zhang, F. Wang, C. Garcia, and R. Kennel, "A very simple strategy for high-quality performance of AC machines using model predictive control," *IEEE Trans. Power Electron.*, vol. 34, no. 1, pp. 794-800, Jan. 2019.
- [25] R. E. K. Meesala, V. P. K. Kuniseti, and V. K. Thippiripati, "Enhanced predictive torque control for open end winding induction motor drive without weighting factor assignment," *IEEE Trans. Power Electron.*, vol. 34, no. 1, pp. 503-513, Jan. 2019.
- [26] Y. Zhang, H. Yang, and B. Xia, "Model predictive control of induction motor drives: torque control versus flux control," *IEEE Trans. Ind Appl.*, vol. 52, no. 5, pp. 4050-4060, Sep. 2016.

- [27] C. A. Rojas, J. Rodriguez, S. Kouro, and F. Villarroel, "Multiobjective fuzzy-decision-making predictive torque control for an induction motor drive," *IEEE Trans. Power Electron.*, vol. 32, no. 8, pp. 6245-6260, Aug. 2017.
- [28] P. Guazzelli, W. Pereira, C. Oliveira, A. Castro, and M. Aguiar, "Weighting factors optimization of predictive torque control of induction motor by multiobjective genetic algorithm," *IEEE Trans. Power. Electron.*, vol. 34, no. 7, pp. 6628-6638, Jul. 2019.
- [29] Y. Zhang, J. Zhu, Z. Zhao, Wei Xu, and D. G. Dorrell, "An improved direct torque control for three-level inverter-fed induction motor sensorless drive," *IEEE Trans. Power. Electron.*, vol. 27, no. 3, pp. 1502-1513, Mar. 2012.
- [30] J. Wang, F. Wang, Z. Zhang, S. Li, and J. Rodriguez, "Design and implementation of disturbance compensation-based enhanced robust finite control set predictive torque control for induction motor systems," *IEEE Trans. Ind Informat.*, vol. 13, no. 5, pp. 2645-2656, Oct. 2017.
- [31] J. Wang, F. Wang, G. Wang, S. Li, and L. Yu, "Generalized proportional integral observer based robust finite control set predictive current control for induction motor systems with time-varying disturbances," *IEEE Trans. Ind Informat.*, vol. 14, no. 9, pp. 4159-4168, Sep. 2018.



Yanqing Zhang (M'19) received the B.S., M.S. and Ph.D. degrees in Electrical Engineering from Xi'an University of Technology, Xi'an, China, in 2012, 2015 and 2019, respectively.

In 2019, he joined the School of Electrical Engineering, Xi'an University of Technology. His main field of interest is high performance control of ac motor.



Zhonggang Yin (M'13) was born in Shandong, China, in 1982. He received the B.S., M.S. and Ph.D. degrees in electrical engineering from Xi'an University of Technology, Shaanxi, China, in 2003, 2006 and 2009, respectively.

In 2009, he joined electrical engineering department of Xi'an University of Technology, where he is currently a professor. His research interests include high performance control of ac motor, and digital control of power converters.



Wei Li was born in Weinan, China, in 1995. She received the B.S. and M.S. degrees in electrical engineering from the Xi'an University of Technology, Xi'an, China, in 2017 and 2020, respectively.

Since 2020, she has been an Engineer with the VEICHI Electric Technology Co., Ltd., Suzhou. Her main research interest is high performance control of ac motors.



Jing Liu was born in Anhui, China, in 1982. She received the B.S., M.S. and Ph.D. degrees in electronic engineering from Xi'an University of Technology, Shaanxi, China, in 2003, 2006 and 2009, respectively.

In 2009, she joined electronic engineering department of Xi'an University of Technology, where she is currently an associate professor. Her research interests include the power semiconductor devices and their application to power electronic devices.



Yanping Xu was born in Henan Province, China, in 1977. She received her B.S. degree from the Xi'an University of Technology, Xi'an, China, in 1999; where she received her M.S. and Ph.D. degrees in Power Electronics and Power Drives, in 2002 and 2008, respectively.

She is presently working as an Associate Professor in the School of Electrical Engineering, Xi'an University of Technology. Her current research interests include power electronics, high performance permanent magnet synchronous motor drives and sensorless control technology.